

# Troublemaker Learning for Low-Light Image Enhancement

Yinghao Song<sup>1,2</sup> Zhiyuan Cao<sup>1,2</sup> Wanhong Xiang<sup>3</sup> Sifan Long<sup>1,2</sup> Hongwei Ge<sup>4</sup> Yanchun Liang<sup>1,2</sup>  
Bo Yang<sup>1,2</sup> Chunguo Wu<sup>1,2</sup>

<sup>1</sup> College of Computer Science and Technology, Jilin University, Jilin, China

<sup>2</sup> Key Laboratory of Symbolic Computation and Knowledge Engineering of Ministry of Education, Jilin University, Jilin, China

<sup>3</sup> YGSOFT INC

<sup>4</sup> Dalian University of Technology

{songyh22, caozy20, longsf22}@mails.jlu.edu.cn, {ycliang, yb, wcg}@jlu.edu.cn,  
xiangwanhong@ygsoft.com, hwge@dlut.edu.cn,

## Abstract

Low-light image enhancement (LLIE) restores the color and brightness of underexposed images. Supervised methods suffer from high costs in collecting low/normal-light image pairs. Unsupervised methods invest substantial effort in crafting complex loss functions. We address these two challenges through the proposed **Troublemaker Learning (TML)** strategy, which employs normal-light images as inputs for training. TML is simple: we first dim the input and then increase its brightness. TML is based on two core components. First, the troublemaker model (TM) constructs pseudo low-light images from normal images to relieve the cost of pairwise data. Second, the predicting model (PM) enhances the brightness of pseudo low-light images. Additionally, we incorporate an enhancing model (EM) to further improve the visual performance of PM outputs. Moreover, in LLIE tasks, characterizing global element correlations is important because more information on the same object can be captured. CNN cannot achieve this well, and self-attention has high time complexity. Accordingly, we propose **Global Dynamic Convolution (GDC)** with  $O(n)$  time complexity, which essentially imitates the partial calculation process of self-attention to formulate elementwise correlations. Based on the GDC module, we build the UGDC model. Extensive quantitative and qualitative experiments demonstrate that UGDC trained with TML can achieve competitive performance against state-of-the-art approaches on public datasets. The code is available at [https://github.com/Rainbowman0/TML\\_LLIE](https://github.com/Rainbowman0/TML_LLIE).

## 1. Introduction

Images taken in low-light environments suffer from underexposure and low contrast. They not only have poor vi-

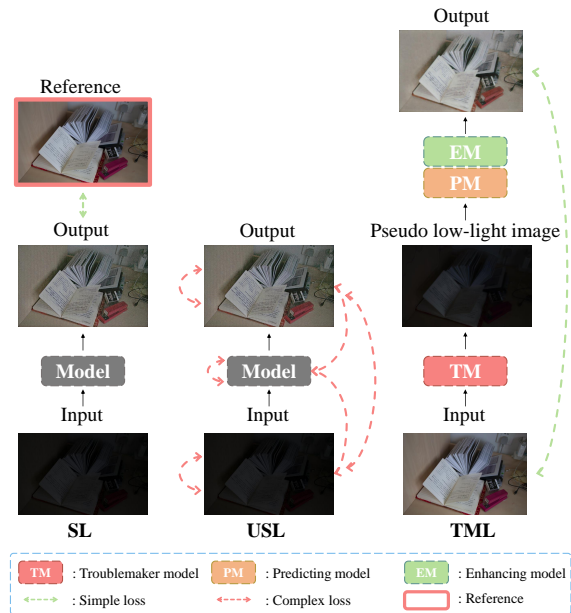


Figure 1. Three categories of training paradigms, SL, USL, and TML, denote supervised learning, unsupervised learning, and troublemaker learning, respectively. Supervised methods rely on paired data, while complex loss functions limit unsupervised methods. TML weakens the paired data restriction and exploits a simple loss function.

sual effects but also create difficulties in downstream visual tasks [27, 62]. Thus, low-light image enhancement (LLIE) aims at improving illumination and producing normal-light images. Traditional methods [2, 24, 26, 40], such as histogram equalization, adjust the contrast at different image locations. Retinex theory divides the image into two parts: illumination and reflection, which represent the lighting in-

formation of the environment and the reflection information of the object, respectively. More studies [14, 23, 24, 38] have utilized the Retinex theory [25] as it aligns with the human eye’s color perception. However, traditional model-based methods require more handcrafted priors, thus restricting their flexibility. Problems such as color distortion and low clarity will occur in many dark-light scenes. With the increase of data volume and computing power, deep learning techniques have become prevalent.

From the perspective of the training paradigm, data-driven methods can be divided into two categories: supervised and unsupervised learning according to whether low/normal image pairs are necessary (SL, USL in Fig. 1). Supervised methods [34, 35, 52, 53, 57, 63] combine outputs and references to calculate a simple loss function. However, it requires paired data and is expensive. Although unsupervised methods [9, 12, 58, 60] remove the paired data restriction, they leverage inputs, outputs and intermediate features to jointly design complex loss functions and introduce many priors. Thus, we ask: *how to design a training paradigm that both alleviates dependence on pairwise data and exploits a simple loss function?*

To answer this question, we propose the TroubleMaker Learning (TML in Fig. 1) strategy. TML is inspired by the adversarial concept of GAN [11] and introduces TM and PM to diminish and enhance image brightness, respectively. Specifically, TM learns the mapping from normal-light to low-light images. PM restores pseudo low-light images generated by TM into coarse normal-light images, and EM further optimizes the PM output in terms of color and brightness. Compared with other supervised and unsupervised methods, the most significant difference of TML is that it takes normal-light images as input, which reduces the reliance on paired data. TML can expand training data at a low cost and exploit a simple loss function. The testing process exclusively involves PM and EM.

In terms of model design, CNN is the most commonly used model structure in LLIE [5, 34, 35, 45, 54]. With the rise of the vision transformer [8], there have been several works [47, 55] using variations of the transformer. As the core transformer component, self-attention can characterize the global element correlations, which will enhance the quantitative and qualitative performance of LLIE methods. Current convolution-based structures cannot capture the correlations. Although vision transformer can achieve this, it has high computational complexity. Thus, we probe a problem: *how to capture elementwise correlations with  $O(n)$  time complexity?*

The proposed Global Dynamic Convolution (GDC in Fig. 2) provides the answer. It is inspired by self-attention. In self-attention, the matrix multiplication of  $Q$  and  $K$  results in attention map  $A$ , whose value represents the relationship between elements at different positions. However,

this calculation process is equivalent to  $1 \times 1$  convolution (Fig. 4). GDC patches the input features and applies them as kernel parameters, which is called dynamic convolution. The output feature obtained by dynamic convolution is similar to attention map  $A$  in self-attention, and its value also represents the elementwise correlations. Compared with other convolution-based models, the most significant advantage of GDC is that it can capture the correlation between elements while maintaining  $O(n)$  time complexity.

Under the guidance of TML, the UGDC model (Fig. 2) we designed based on GDC achieved competitive results against the state-of-the-art approaches on public datasets. In summary, the contributions of our work are as follows:

- We propose the TML strategy that alleviates the dependence on pairwise data and complex priors.
- We propose a novel convolution module GDC, which can capture the correlation between long-distance elements with  $O(n)$  time complexity.
- We conduct extensive qualitative, quantitative, and visual experiments to demonstrate the effectiveness of TML and GDC.

## 2. Related work

### 2.1. Learning-based methods

**Supervised methods.** LLNet [32] used MLP to lighten grayscale images. MBLLN [34] proposed using CNN and multibranch structure to process low-light images. Chen *et al.* [5] first applied the U-Net structure to the LLIE field and achieved exciting results. Jiang *et al.* [21] dedicated to solving motion blur in low-light videos. Xu *et al.* [54] proposed to learn low-frequency and high-frequency information and then added the two to obtain the prediction result. DLN [45] proposed learning “brightness residuals”. The normal-light image was equal to the sum of the brightness residuals and the low-light image. Lv *et al.* [35] introduced exposure and noise attention to improve the prediction performance. Xu *et al.* [55] exploited CNN and transformer to model short-range and long-range dependencies simultaneously. LLFormer [47] designed the height and width axis attention to replace the multihead self-attention. Xu *et al.* [57] used the edge structure information of the image to obtain a clearer normal-light image.

In addition, there are some works based on Retinex theory. Retinex-Net [52] exploited Retinex theory earlier and proposed learning reflection and illumination. Lighten-Net [28] and DeepUPE [46] predicted the illumination of low-light images and then leveraged reflection as normal-light images. KinD [64] used a set of different exposure images instead of low-light and normal-light images during training. Recent works such as URetinex-Net [53] designed

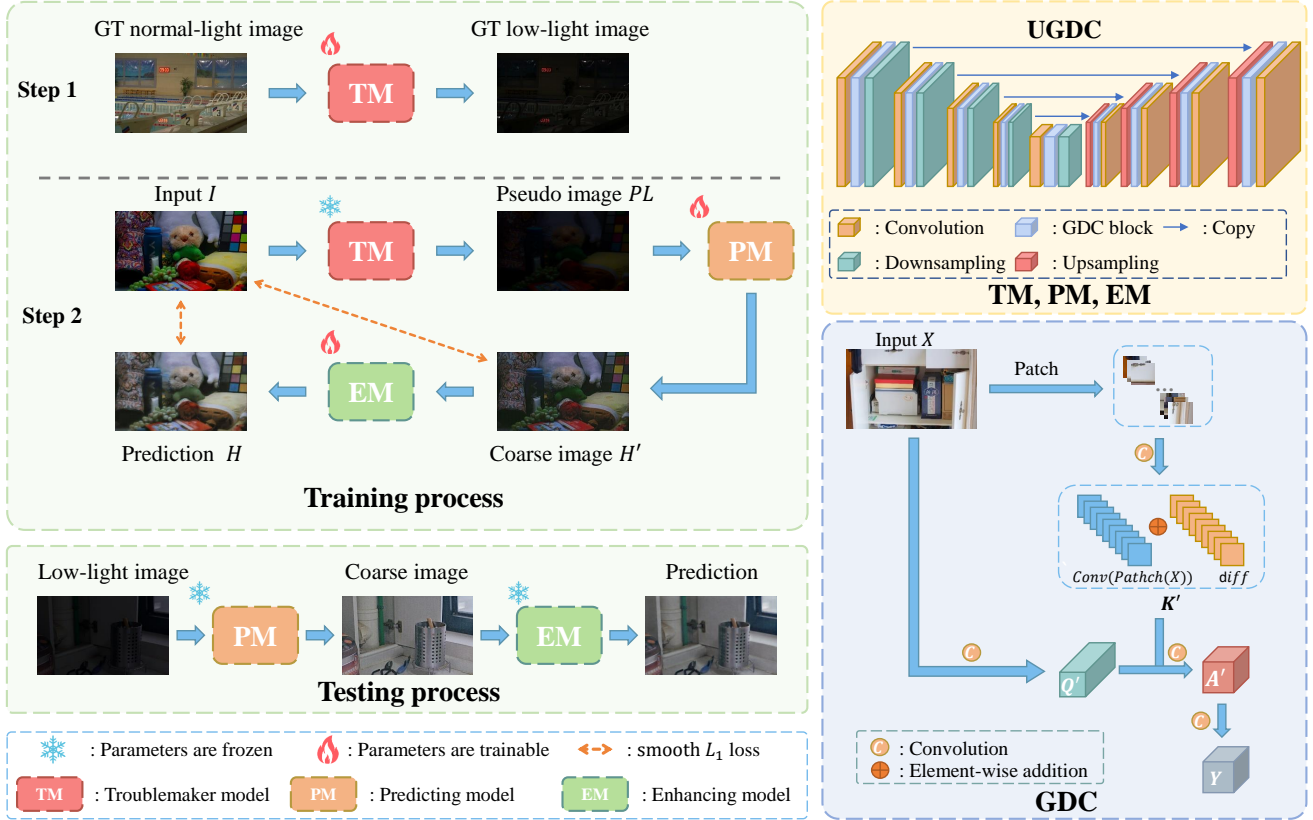


Figure 2. Overview of TML. The left side shows the TML training and testing process. In the training phase, TM only serves as a pseudo label generator. Step 1 requires a small quantity of paired data for training TM. Step 2 freezes TM and trains only PM and EM. The testing phase involves PM and EM. The UGDC (TM, PM and EM structure) and GDC details are on the right. GDC imitates the partial calculation process of self-attention and corresponds with Eqs. (8) to (11).

the initialization module so that the illumination and reflection initialization values are input-adaptive.

However, supervised methods require higher costs to collect paired data, so it is difficult to expand the training data.

**Unsupervised methods.** Unsupervised methods break the constraints of paired data. Inspired by the image processing software Photoshop, ExCNet [60] proposed learning "S-curve". ZeroDCE [12] was similar to ExCNet and guided the model to learn a more refined "S-curve". EnlightenGAN [22] exploited U-Net as a generator and used a double discriminator to learn global and local information. RUAS [29] established models to characterize the intrinsic underexposed structure of low-light images. RRDNet [65] decomposed the image into three parts: illumination, reflection and noise to achieve a better denoising effect. Recent works such as SCI [36] established a cascaded illumination learning process with weight sharing. NeRCO [58] introduced the idea of multimodality into LLIE for the first time. PairLIE [9] was based on Retinex theory and leveraged pairs of low-light images to train the model. It achieved

competitive results. However, these works rely heavily on redundant loss functions to ensure convergence. They introduce many priors, which limits their generalization ability.

## 2.2. CNN backbones

U-Net is the most commonly used backbone in LLIE. It was first applied in biomedical image segmentation [41]. There is a series of works [21, 22, 34, 35, 47, 51, 52, 54, 57, 59] that exploited U-Net-like structures as part of the model structure.

U-Net performs well in many fields because it integrates low/mid/high-level features. In fact, there are many excellent CNN structures in addition to U-Net. ResNet [16] first proposed using CNN to learn residuals. This idea was widely used in various fields. Inception [44] decomposed the convolution kernels so that the model had receptive fields of different sizes. DenseNet [19] is an extension of ResNet that proposed denser residual connections. MobileNet [17] leveraged depthwise and pointwise convolutions, greatly reducing the number of parameters and inference time. SENet [18] introduced the global atten-

tion mechanism into CNN and achieved competitive results. ConvNeXt [31] optimized the original ResNet by imitating the model structure and training strategy of Swin Transformer [30]. It proved that the potential of CNN has not been fully explored. Recent works such as DeepMAD [43] proposed a pure mathematical framework to maximize network entropy. FasterNet [6] designed partial convolution to reduce redundant information between channels. Xu *et al.* [55] and Wang *et al.* [47] illustrated that characterizing long-distance elementwise correlations are helpful in LLIE. Some efforts use convolution kernels for global attention to model long-range dependencies. RepLKNet [7] enlarges the kernel size to 31x31. VAN [13] employs depth-wise convolution, depth-wise dilation convolution, and pointwise convolution to expand the receptive field while reducing computational complexity. In contrast, GDC uses image patches as convolution kernel parameters to mimic Q-K multiplication in self-attention, thereby integrating global attention.

### 3. Method

In this section, we first introduce TML, including motivation, overall process, and detailed analysis. The GDC is then presented, including motivation and design details.

#### 3.1. Troublemaker learning

**Motivation.** TML is inspired by the adversarial concept from GAN [11] and introduces the "bad student" (*i.e.* TM) and "good student" (*i.e.* PM). Specifically, TM intentionally learns a poor feature, which is a pseudo low-light image based on a normal-light input. The pseudo low-light image serves as a pseudo label for subsequent training. In contrast, PM learns the mapping from low-light to normal-light images, enhancing image brightness.

**TML overall process.** The TML pipeline is illustrated in Fig. 2. The training process consists of two steps. Step 1 is to obtain a pseudo low-light image generator; thus, a small number of low/normal image pairs are required to train TM. It is worth noting that we use normal-light images as inputs and low-light images as labels. The input of step 2 is a normal-light image  $I$ . TM first reduces its brightness to generate a pseudo low-light image  $PL$ . Then, PM increases the  $PL$  brightness to obtain a coarse normal-light image  $H'$ . Finally, EM further optimizes the brightness and color of  $H'$  to obtain normal-light prediction  $H$ . In step 2, we freeze TM, update the PM and EM parameters, and the test process includes only PM and EM. TM, PM, and EM all employ the UGDC network architecture (top right of Fig. 2).

We consider two EM design options. In one option, EM directly predicts the mapping from  $H'$  to  $H$ :

$$H = EM(H') \quad (1)$$

The other option predicts the residual between  $H'$  and  $H$ , prediction  $H$  is the difference between  $H'$  and the residual:

$$residual = EM(H') \quad (2)$$

$$H = H' - residual \quad (3)$$

Ablation experiments confirmed that the latter performs better; details are shown in Tab. 3. In step 2, PM and EM are trained separately. The distance between  $H'$  and  $I$  and between  $H$  and  $I$  is measured by the  $smooth_{\mathcal{L}_1}$  [10] loss function:

$$\mathcal{L} = \frac{1}{n} \sum_i smooth_{\mathcal{L}_1}(y_i, h_i) \quad (4)$$

$$smooth_{\mathcal{L}_1}(y_i, h_i) = \begin{cases} 0.5(y_i - h_i)^2 & \text{if } |y_i - h_i| < 1 \\ |y_i - h_i| - 0.5 & \text{otherwise} \end{cases} \quad (5)$$

where  $y_i$  is the element in the input  $I$  in step 2,  $h_i$  represents the element in  $H$  and  $H'$ , and  $n$  represents the number of pixels. For a  $400 \times 640$  RGB image,  $n = 400 \times 640 \times 3 = 768,000$ .

**TML alleviates reliance on pairwise data.** Although step 1 still requires paired data, experiments have proven that a good pseudo low-light generator can be obtained with only 200 pairwise data (Tab. 2). The testing process includes only PM and EM. It is worth noting that only normal-light images are used when training both, which greatly weakens the paired data constraints. Therefore, the training data can be expanded at a low cost to improve the generalization of the model.

Like most deep learning methods, TML is data-driven. Previous studies have shown that data-driven techniques can create realistic normal-light images from low-light RGB images. Thus, we believe TM can similarly produce realistic low-light images from normal-light RGB images. Tab. 2 demonstrates the similarity in data distribution between TM-generated and real low-light images. The prediction results of TM are illustrated in Fig. 3. Traditional supervised methods exploit low/normal-light image pairs. To ensure the same semantic information, a common approach is to obtain two images with different exposures via adjusting the camera ISO [15, 52]. However, this sometimes does not guarantee the consistency of semantic information. As shown in the fourth row of Fig. 3, we find that the sky colors of low-light and normal-light images are different because low-light images have lower ISO and, therefore, retain more color details. TML can address this issue. The two have stronger semantic consistency because pseudo low-light images are directly predicted by normal-light images. In addition, we observe that TML predictions

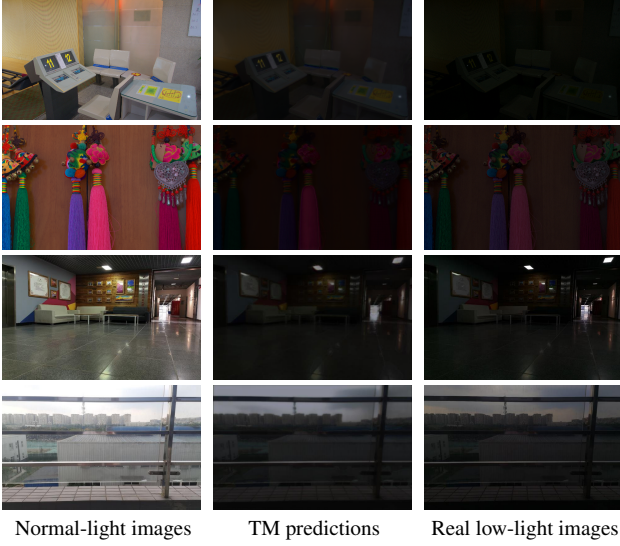


Figure 3. Pseudo low-light images. The first and third columns are normal-light and real low-light images obtained via adjusting ISO. The second column is the pseudo low-light images predicted by TM.

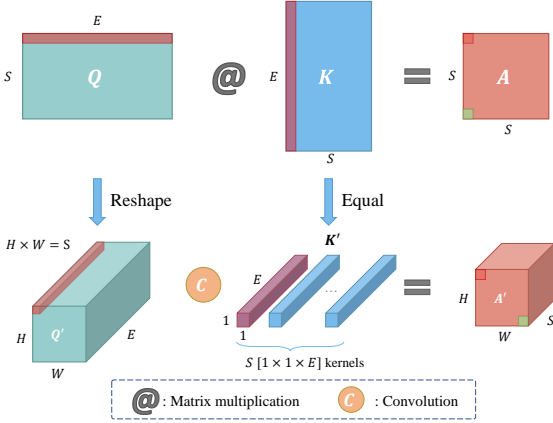


Figure 4. The matrix multiplication between  $Q$  and  $K$  in self-attention (top) can be replaced by a convolution operation (bottom). We use red and green to mark the equivalent elements in  $Q$  and  $Q'$ ,  $K$  and  $K'$ ,  $A$  and  $A'$ .

are more blurry than real low-light images. This is equivalent to a data augmentation strategy, so the trained model is more robust.

### 3.2. Global dynamic convolution

**Motivation.** CNN has inductive biases such as locality and translation invariance and retains the 2D image structure information. However, it cannot capture element-wise correlations. Vision transformers can achieve this; however, the computational complexity is high. Recent works [47, 55] have demonstrated that characterizing corre-

lations between elements improves model performance for darker regions.

**Global dynamic convolution.** The self-attention calculation process can be expressed by:

$$A = Q \times K^T \quad (6)$$

$$Y = \text{softmax}\left(\frac{A}{\sqrt{d_k}}\right) \times V \quad (7)$$

where  $Q$ ,  $K$  and  $V$  are attained by the linear transformation of the input.  $A$  refers to attention map, which represents the correlations between elements at different positions.  $d_k$  represents the dimensions of  $K$ .

GDC applies convolution to imitate Eq. (6). As illustrated in Fig. 4, we reshape  $Q$  into a 3-dimensional feature map  $Q'$ , and regard  $K$  as  $K'$ , which contains  $S \times 1 \times E$  kernels. Accordingly, matrix multiplication between  $Q$  and  $K$  is equivalent to convolution between  $Q'$  and  $K'$ . Each element of  $A'$  also represents the correlation between different elements of  $Q'$  and  $K'$ .

It is worth noting that in self-attention, parameters  $Q$  and  $K$  are input-adaptive. However, if we regard  $K'$  as  $S \times 1 \times E$  kernels, the parameters of  $K'$  are fixed. To address this, we propose GDC block (the right part of Fig. 2).

The calculation process of GDC can be expressed as

$$K' = \text{Conv}(\text{Patch}(X)) + \text{diff} \quad (8)$$

$$Q' = \text{Conv}(X) \quad (9)$$

$$A' = \text{Conv}_{K'}(Q') \quad (10)$$

$$Y = \text{Conv}(A') \quad (11)$$

where  $\text{Conv}_{K'}(Q')$  means applying  $K'$  as the convolution kernels and convolving with  $Q'$ .  $\text{Patch}$  refers to breaking the image into small patches, and  $\text{diff}$  refers to the trainable parameters.

GDC first patches the input  $X$  and then performs convolution. The obtained result is added to the trainable parameter  $\text{diff}$  to increase the nonlinearity of  $K'$ .  $K'$  and  $Q'$  are convolved to obtain  $A'$ . The result  $Y$  is obtained by convolution transformation of  $A'$ . We replaced several convolutional layers in U-Net [41] with GDC block and designed UGDC (the right part of Fig. 2).

**Advantages of GDC.** GDC applies convolution to imitate the matrix multiplication process of  $Q$  and  $K$  in self-attention. Therefore, unlike previous convolutional modules, GDC can capture the element-wise correlations between long-distance (Fig. 8) and the parameters are input-adaptive. In addition, the time complexity of self-attention is  $O(n^2)$ , while GDC is  $O(n)$ , which means that the time complexity increases linearly as the image size increases, so it is more economical.

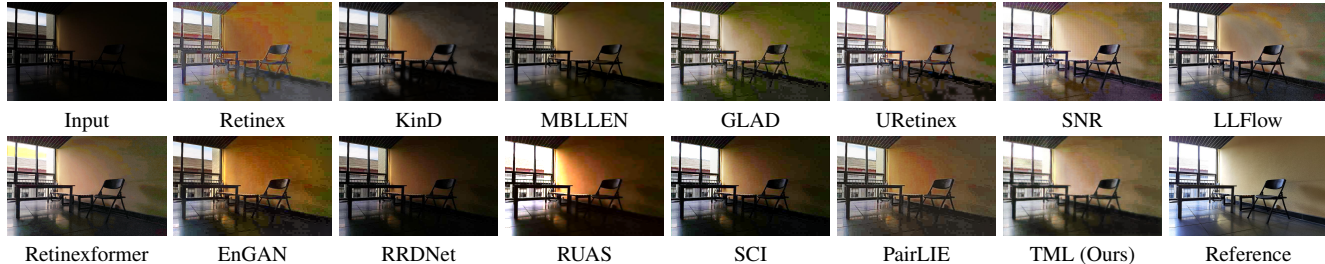


Figure 5. Qualitative comparisons with state-of-the-art methods. TML makes reasonable trade-offs in brightness, color, and image quality.

Method	Type	LSRW				LOL				RELLISUR			
		PSNR $\uparrow$	SSIM $\uparrow$	LPIPS $\downarrow$	NIQE $\downarrow$	PSNR $\uparrow$	SSIM $\uparrow$	LPIPS $\downarrow$	NIQE $\downarrow$	PSNR $\uparrow$	SSIM $\uparrow$	LPIPS $\downarrow$	NIQE $\downarrow$
Retinex [52]	S	15.885	0.652	0.388	5.652	17.575	0.775	0.382	4.201	15.945	0.289	0.532	4.643
KinD [63]	S	16.989	0.674	0.330	4.659	17.755	0.841	0.176	4.411	16.307	0.304	0.425	3.948
MBLEEN [34]	S	16.930	0.663	0.342	5.341	17.857	0.790	0.226	4.395	16.673	0.429	0.400	4.187
GLAD [48]	S	18.763	0.725	0.306	4.524	19.743	0.805	0.327	5.510	16.636	0.349	0.472	4.050
URetinex [53]	S	17.682	0.702	0.303	4.875	20.162	<b>0.876</b>	0.131	4.253	18.221	0.401	0.332	5.632
SNR [56]	S	17.733	0.626	0.234	4.347	24.639	0.861	<b>0.114</b>	4.840	17.791	0.384	0.387	5.559
LLFlow [49]	S	17.976	0.621	<b>0.213</b>	<b>3.878</b>	20.941	0.863	0.117	5.662	18.429	0.389	0.337	4.136
Retinexformer [4]	S	18.201	0.613	0.220	3.912	<b>21.794</b>	0.858	0.130	<b>3.805</b>	18.810	0.342	<b>0.317</b>	4.876
EnGAN [22]	U	17.854	0.699	0.330	4.274	17.595	0.772	0.331	4.247	17.063	0.362	0.448	4.485
RRDNet [65]	U	13.494	0.542	0.338	6.082	11.350	0.545	0.370	6.241	10.867	0.163	0.505	4.841
RUAS [29]	U	14.467	0.634	0.434	6.810	16.430	0.658	0.275	5.879	13.738	0.265	0.428	5.050
SCI [36]	U	15.604	0.615	0.315	5.329	14.807	0.652	0.351	6.419	12.078	0.212	0.446	<b>3.458</b>
PairLIE [9]	U	18.137	0.720	0.324	5.338	18.499	0.835	0.248	4.031	17.241	0.360	0.328	4.137
<b>TML (ours)</b>	T	<b>19.358</b>	<b>0.743</b>	0.360	4.727	20.780	0.820	0.303	5.311	<b>19.444</b>	<b>0.460</b>	0.351	5.318

Table 1. Quantitative comparisons with state-of-the-art methods on LOL and LSRW datasets. "U", "S", and "T" represent supervised learning, unsupervised learning and troublemaker learning respectively.  $\uparrow$  represents that the larger the value, the more similar the prediction and reference are in color and brightness.  $\downarrow$  represents that the smaller the value, the better the image quality.

## 4. Experiments

We first describe the implementation details, datasets, metrics and compared methods. Then, the quantitative and qualitative comparisons with existing methods are presented. We then conduct ablation experiments to prove the effectiveness of the design. We also perform visualization studies to demonstrate the explicability of TML and GDC. Finally, the limitations of our work are discussed. All experiments are completed on the NVIDIA 2080Ti GPU under PyTorch [39] framework.

### 4.1. Experimental settings

**Implementation details.** In the training phase, we use the AdamW [33] optimizer and the learning rate is set to  $4e-5$ . The loss function is  $smooth_{\mathcal{L}_1}$ . TM and PM are trained for 15 epochs, and EM is trained for 30 epochs. The input size is  $400 \times 640$  and the batch size is set to 8. We do not apply complex training techniques to verify the effectiveness of TML and GDC. The training process of both PM and EM exclusively utilizes normal-light images.

**Datasets and metrics.** TM and EM are trained on LSRW [15]. In step 2, PM is trained on the BIGGER dataset we collected. The testing process is carried out on

LSRW and LOL [52]. LSRW contains 5,600 low/normal-light image pairs for training and 50 pairs for testing. LOL has 485 and 15 pairs of data for training and testing, respectively. We select a total of 11,663 normal-light images from LSRW, SICE [3], DPED [20], and RELLISUR [1] to construct the BIGGER dataset. We employ peak signal-to-noise ratio (PSNR), structural similarity (SSIM) [50], learned perceptual image patch similarity (LPIPS) [61], natural image quality evaluator (NIQE) [37] to measure the effectiveness of the model. A higher PSNR/SSIM indicates the prediction is closer to the reference in color and brightness. The lower the LPIPS/NIQE, the higher the predicted image quality.

**Compared methods.** We compare 13 recent state-of-the-art methods, including 8 supervised and 5 unsupervised methods. Supervised methods include Retinex-Net [52], MBLEEN [34], GLADNet [48], KinD [63], URetinex-Net [53], SNR [56], LLFlow [49], Retinexformer [4] and unsupervised methods include EnlightenGAN [22], RRDNet [65], RUAS [29], SCI [36], PairLIE [9]. We use the officially provided codes and pretrained parameters for testing. To ensure fairness, the image sizes are all  $400 \times 640$ . All comparisons are completed on an NVIDIA 2080Ti GPU.

## 4.2. Quantitative comparisons

Tab. 1 lists the quantitative evaluation results on the LOL, LSRW and RELISUR [1] datasets. RELISUR contains real low-light images for super-resolution. We chose 85 paired data from the validation set for testing. We can observe that the overall numerical performance of unsupervised methods is inferior to that of supervised methods. In the absence of references, unsupervised methods depend on priors such as complex loss functions to ensure model convergence, leading to limited generalization. In comparison, TML achieves competitive results. TML’s good performance is attributed to the following two aspects. First, TML applies only normal-light images in step 2, which alleviates the dependence on paired data. Therefore, the training data can be easily expanded to improve the effect. Second, GDC can capture the correlations between elements over a larger area. UGDC can better capture semantic features in darker areas. TML excels in PSNR and SSIM on the LSRW and RELISUR datasets, while Retinexformer performs better on LOL. We also observe that although TML performs competitively on PSNR and SSIM, it is suboptimal on LPIPS and NIQE. This proves that the prediction results perform well in terms of brightness and color, but there is room for improvement in image quality.

## 4.3. Qualitative comparisons

Fig. 5 shows qualitative comparisons between TML and other state-of-the-art methods. In terms of brightness, supervised methods are brighter overall than unsupervised methods. This is due to the high brightness of references in training data such as LOL and LSRW, so supervised methods can easily learn this brightness mapping. However, unsupervised methods lack reference guidance and rely on handcrafted priors to learn similar mappings, which is more difficult and lacks adaptability. TML is competitive in brightness because the input to step 2 is normal-light images, which means higher brightness is provided as a reference during the training stage. In terms of image quality, we observe that methods with good brightness and color performance do not necessarily have high image quality. Some methods (MBLLEN [34], RRDNet [65], SCI [36]) have mediocre brightness performance but higher image quality. TML makes trade-offs in brightness, color, and image quality. By slightly reducing image quality, it greatly improves brightness and color performance, as detailed in the ablation experiments.

## 4.4. Ablation study

We trained the TM with varying scales of paired data from LSRW. Notably, we compared the gap between TM’s outputs and real low-light images. Tab. 2 shows that training TM with just 200 pairs yields outputs close to real low-light images. More paired training data does not significantly

Method	LOL				LSRW			
	PNSR↑	SSIM↑	LPIPS↓	NIQE↓	PNSR↑	SSIM↑	LPIPS↓	NIQE↓
200	25.645	0.701	0.226	<b>6.155</b>	<b>27.962</b>	<b>0.730</b>	<b>0.190</b>	7.384
400	25.355	0.718	0.226	6.396	25.109	0.723	0.220	7.053
1600	<b>27.512</b>	<b>0.753</b>	0.219	6.477	25.269	0.727	0.242	<b>6.915</b>
3200	25.001	0.686	0.229	6.537	24.083	0.676	0.256	7.469
5650	27.376	0.742	<b>0.205</b>	6.591	25.588	<b>0.730</b>	0.222	7.586

Table 2. TM’s ablation study on the LSRW dataset. TM trained with only 200 paired data produces outputs close to real low-light images.

ID	TM	PM	EM		LOL			
	w/ GDC	w/ GDC	w/ GDC	w/ res	PNSR↑	SSIM↑	LPIPS↓	NIQE↓
A					16.823	0.732	0.405	5.434
B				✓	19.072	0.814	0.323	5.315
C	✓			✓	19.201	0.812	0.332	6.202
D		✓		✓	19.301	0.806	0.335	5.716
E			✓	✓	20.622	0.820	<b>0.294</b>	<b>4.792</b>
F	✓	✓	✓		20.733	0.818	0.410	6.041
G	✓	✓	✓	✓	<b>20.780</b>	<b>0.820</b>	0.303	5.311

Table 3. Quantitative results of ablation studies on the LOL dataset. The best results are shown in bold. ✓ in w/ GDC refers to adding GDC to U-Net, that is, using the UGDC model. Otherwise, U-Net is used. ✓ in w/ res indicates that EM predicts the *residual* between  $H$  and  $H'$  in Eq. (2), rather than mapping from  $H'$  to  $H$  in Eq. (1).

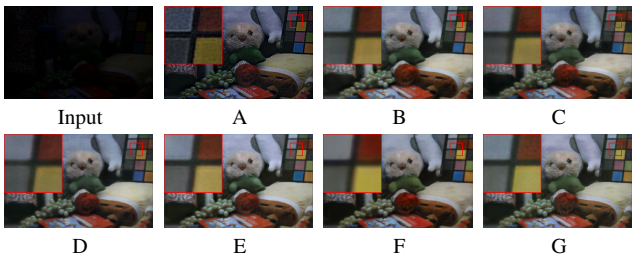


Figure 6. Visual comparisons of the ablation studies. Setting G achieves competitive performance in color, brightness and image quality.

improve performance and may even reduce the quality of TM’s predicted pseudo low-light images. Therefore, we ultimately selected 200 paired images from LSRW to train TM.

To verify the effectiveness of TML design, we conduct extensive ablation experiments, as shown in Tab. 3. In setting A, TM and PM use U-Net without GDC, and EM is removed. In setting B, TM, PM and EM all adopt U-Net. C, D, and E add GDC in TM, PM, and EM, respectively. In addition, EM from settings B to E all predict the residuals from  $H'$  to  $H$  in Eq. (2). Setting F adds GDC to TM, PM and EM. EM predicts a direct mapping of  $H'$  to  $H$  in Eq. (1). Setting G is what we ultimately adopted.

Comparing A and B, we observe that EM greatly improves the prediction performance in color, brightness (PSNR, SSIM) and image quality (LPIPS, NIQE). The comparison between B, C, D, and E proves that adding GDC

Dataset	Size	PSNR $\uparrow$	SSIM $\uparrow$	LPIPS $\downarrow$	NIQE $\downarrow$
LOL	485	19.880	0.805	0.313	5.789
LSRW	5600	20.546	0.817	0.312	5.634
BIGGER	11663	<b>20.780</b>	<b>0.820</b>	<b>0.303</b>	<b>5.311</b>

Table 4. Results for different sized datasets. Only normal-light images are used in the training phase. The results are obtained on the LOL test set. The best results are in bold.

	URetinex [53]	SNR [56]	Retinexformer [4]	PairLIE [9]	TML (ours)
FLOPs(G)	227.631	90.425	66.478	87.294	<b>58.670</b>
Params(M)	0.360	3.104	1.606	<b>0.342</b>	4.442

Table 5. Model FLOPs and parameter count comparison.

to each model will improve the prediction performance in terms of color and brightness, proving the effectiveness of GDC and illustrating that capturing the correlation between elements is necessary for LLIE. Interestingly, adding GDC to TM and PM degrades LPIPS and NIQE, while adding it to EM improves LPIPS and NIQE, which indicates that GDC may slightly reduce sharpness. Setting G is slightly higher than F in PSNR and SSIM but has a larger improvement in LPIPS and NIQE. Although G is slightly lower than E in image quality, it performs better in color and brightness. According to a comprehensive comparison of settings A to G, we conclude that G makes a reasonable trade-off in color, brightness, and image quality. We visualize the predictions for settings A to G as illustrated in Fig. 6. The visual effect of A is poor. B, C, D, and F are average in terms of clarity. In comparison, the visual effect of G is slightly better than that of E, which is consistent with the previous analysis.

Because TML can easily increase training data, we exploit different sized datasets in step 2 during the training phase. The results are listed in Tab. 4. We observe that using larger datasets leads to better numerical results, proving that TML can improve prediction performance in color, brightness and image quality by increasing training data at a low cost. It is worth noting that although BIGGER does not contain LOL training data, it achieves the best performance on the LOL test set, indicating that TML has good generalization properties. All datasets exploit normal-light images.

#### 4.5. FLOPs and parameters

As shown in Eqs. (8) to (11), GDC essentially conducts convolution operations with image patches as kernel parameters, thus its time complexity remains  $O(n)$ . We compared TML’s FLOPs and parameter count with several SOTA methods, shown in Tab. 5 (image size is  $400 \times 640$ ). It is evident that TML has an advantage in FLOPs, indicating its computational efficiency. However, PairLIE [9] is more lightweight in terms of parameter count.

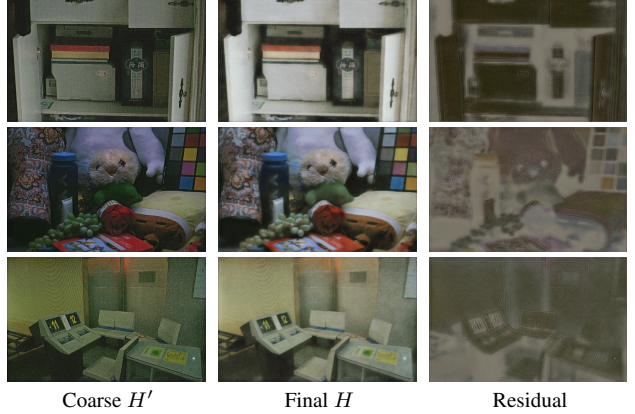


Figure 7. EM predictions. The first, second, and third columns represent  $H'$ ,  $H$ , and  $residual$ , respectively, in Eqs. (2) and (3).

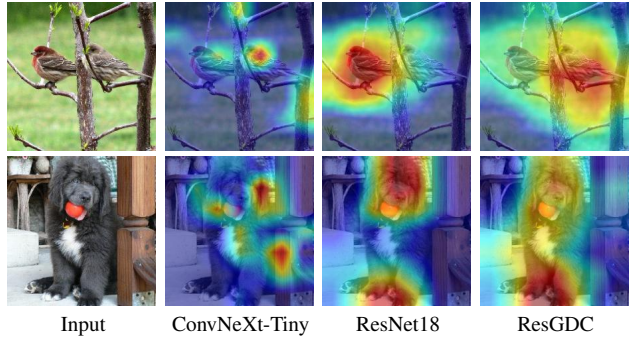


Figure 8. Grad-CAM for ConvNeXt-Tiny, ResNet18 and ResGDC. ResGDC can capture the correlation between a wider range of elements, indicating that GDC can improve the convolution module’s ability to depict global element correlation.

#### 4.6. Visualization study

**Brightness residual.** We visualize the brightness residual predicted by EM as illustrated in Fig. 7. The first, second, and third columns represent  $H'$ ,  $H$ , and  $residual$ , respectively, in Eqs. (2) and (3). We observe that the  $residual$  predicted by EM is an adaptive brightness map. Instead of brightening all elements of  $H'$ , it brightens the parts that should be brightened without changing the brightness of the remaining parts.

**GDC captures the correlations between elements on a larger scale.** We replace the convolutional layers of the last two layers in ResNet18 [16] with GDC to form ResGDC. We then use the mini-ImageNet to train ConvNeXt-Tiny [31], ResNet18 and ResGDC with similar parameters and visualize their Grad-CAM [42], as shown in Fig. 8. We observe that although ConvNeXt-Tiny performs better on ImageNet classification, it cannot characterize the correlations between elements well. Compared with ResNet18, ResGDC can capture a wider range of element correlations

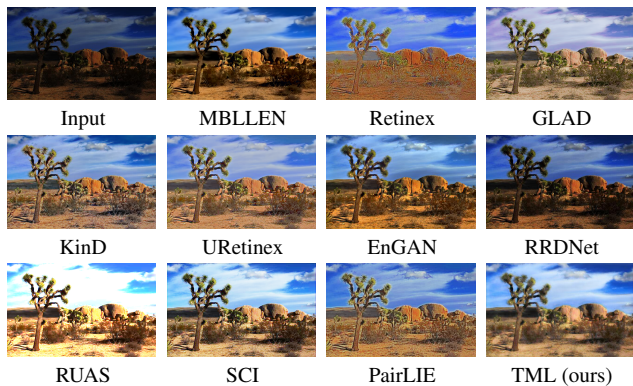


Figure 9. Performance of different methods on SICE dataset. TML has room for improvement in terms of sharpness and clarity.

at the individual level. For instance, ResNet18 can capture information about only one bird, while ResGDC can capture information about two birds.

#### 4.7. Discussion

**Limitations.** TML has room for improvement in two aspects. First, despite alleviating the reliance on paired data, step 1 of TML still requires a small number of low/normal image pairs to train the pseudo low-light image generator. If the TM training process abandons paired data or uses an existing pretrained model as a pseudo low-light image generator, TML can be completely freed from the paired data limitations. Second, based on previous comparative experiments, we observe the TML image quality can still be optimized. Fig. 9 shows the performance of different methods on the SICE [3] dataset. All methods have not been trained on this dataset. Although TML can obtain competitive visual effects, its sharpness and clarity are average.

**Future work.** The idea of TML is universal and can be applied to other scenarios that require paired data. In addition, GDC can capture correlations between a larger range of elements, so it can be applied in other general vision tasks. After solving the above two limitations, we will apply TML and GDC to other vision tasks.

#### 5. Conclusion

In this paper, we address two questions raised previously: First, we propose a training strategy called Trouble-Maker Learning (TML). TML employs TM and PM separately to decrease and increase image luminance, and training data can be easily increased to improve the effect. It alleviates the dependence on pairwise data and uses a simple loss function. Second, we propose the Global Dynamic Convolution (GDC) module. GDC can capture element-wise correlations in a wide range with  $O(n)$  time complexity. Extensive quantitative and qualitative experiments

demonstrate the effectiveness of TML and GDC.

#### References

- [1] Andreas Aakerberg, Kamal Nasrollahi, and Thomas B Moeslund. Rellisur: a real low-light image super-resolution dataset. In *Thirty-fifth Conference on Neural Information Processing Systems Datasets and Benchmarks Track (Round 2)*, 2021. 6, 7
- [2] Mohammad Abdullah-Al-Wadud, Md Hasanul Kabir, M Ali Akber Dewan, and Oksam Chae. A dynamic histogram equalization for image contrast enhancement. *IEEE transactions on consumer electronics*, 53(2):593–600, 2007. 1
- [3] Jianrui Cai, Shuhang Gu, and Lei Zhang. Learning a deep single image contrast enhancer from multi-exposure images. *IEEE Transactions on Image Processing*, 27(4):2049–2062, 2018. 6, 9
- [4] Yuanhao Cai, Hao Bian, Jing Lin, Haoqian Wang, Radu Timofte, and Yulun Zhang. Retinexformer: One-stage retinex-based transformer for low-light image enhancement. *arXiv preprint arXiv:2303.06705*, 2023. 6, 8
- [5] Chen Chen, Qifeng Chen, Jia Xu, and Vladlen Koltun. Learning to see in the dark. In *Proceedings of the IEEE conference on computer vision and pattern recognition*, pages 3291–3300, 2018. 2
- [6] Jierun Chen, Shiu-hong Kao, Hao He, Weipeng Zhuo, Song Wen, Chul-Ho Lee, and S-H Gary Chan. Run, don’t walk: Chasing higher flops for faster neural networks. In *Proceedings of the IEEE/CVF Conference on Computer Vision and Pattern Recognition*, pages 12021–12031, 2023. 4
- [7] Xiaohan Ding, Xiangyu Zhang, Jungong Han, and Guiguang Ding. Scaling up your kernels to 31x31: Revisiting large kernel design in cnns. In *Proceedings of the IEEE/CVF conference on computer vision and pattern recognition*, pages 11963–11975, 2022. 4
- [8] Alexey Dosovitskiy, Lucas Beyer, Alexander Kolesnikov, Dirk Weissenborn, Xiaohua Zhai, Thomas Unterthiner, Mostafa Dehghani, Matthias Minderer, Georg Heigold, Sylvain Gelly, et al. An image is worth 16x16 words: Transformers for image recognition at scale. *arXiv preprint arXiv:2010.11929*, 2020. 2
- [9] Zhenqi Fu, Yan Yang, Xiaotong Tu, Yue Huang, Xinghao Ding, and Kai-Kuang Ma. Learning a simple low-light image enhancer from paired low-light instances. In *Proceedings of the IEEE/CVF Conference on Computer Vision and Pattern Recognition*, pages 22252–22261, 2023. 2, 3, 6, 8
- [10] Ross Girshick. Fast r-cnn. In *Proceedings of the IEEE international conference on computer vision*, pages 1440–1448, 2015. 4
- [11] Ian Goodfellow, Jean Pouget-Abadie, Mehdi Mirza, Bing Xu, David Warde-Farley, Sherjil Ozair, Aaron Courville, and Yoshua Bengio. Generative adversarial nets. *Advances in neural information processing systems*, 27, 2014. 2, 4
- [12] Chunle Guo, Chongyi Li, Jichang Guo, Chen Change Loy, Junhui Hou, Sam Kwong, and Runmin Cong. Zero-reference deep curve estimation for low-light image enhancement. In

- Proceedings of the IEEE/CVF conference on computer vision and pattern recognition*, pages 1780–1789, 2020. 2, 3
- [13] Meng-Hao Guo, Cheng-Ze Lu, Zheng-Ning Liu, Ming-Ming Cheng, and Shi-Min Hu. Visual attention network. *Computational Visual Media*, 9(4):733–752, 2023. 4
- [14] Xiaojie Guo, Yu Li, and Haibin Ling. Lime: Low-light image enhancement via illumination map estimation. *IEEE Transactions on image processing*, 26(2):982–993, 2016. 2
- [15] Jiang Hai, Zhu Xuan, Ren Yang, Yutong Hao, Fengzhu Zou, Fang Lin, and Songchen Han. R2rnet: Low-light image enhancement via real-low to real-normal network. *Journal of Visual Communication and Image Representation*, 90: 103712, 2023. 4, 6
- [16] Kaiming He, Xiangyu Zhang, Shaoqing Ren, and Jian Sun. Deep residual learning for image recognition. In *Proceedings of the IEEE conference on computer vision and pattern recognition*, pages 770–778, 2016. 3, 8
- [17] Andrew G Howard, Menglong Zhu, Bo Chen, Dmitry Kalenichenko, Weijun Wang, Tobias Weyand, Marco Andreetto, and Hartwig Adam. Mobilenets: Efficient convolutional neural networks for mobile vision applications. *arXiv preprint arXiv:1704.04861*, 2017. 3
- [18] Jie Hu, Li Shen, and Gang Sun. Squeeze-and-excitation networks. In *Proceedings of the IEEE conference on computer vision and pattern recognition*, pages 7132–7141, 2018. 3
- [19] Gao Huang, Zhuang Liu, Laurens Van Der Maaten, and Kilian Q Weinberger. Densely connected convolutional networks. In *Proceedings of the IEEE conference on computer vision and pattern recognition*, pages 4700–4708, 2017. 3
- [20] Andrey Ignatov, Nikolay Kobyshev, Radu Timofte, Kenneth Vanhoey, and Luc Van Gool. Dslr-quality photos on mobile devices with deep convolutional networks. In *Proceedings of the IEEE international conference on computer vision*, pages 3277–3285, 2017. 6
- [21] Haiyang Jiang and Yinqiang Zheng. Learning to see moving objects in the dark. In *Proceedings of the IEEE/CVF International Conference on Computer Vision*, pages 7324–7333, 2019. 2, 3
- [22] Yifan Jiang, Xinyu Gong, Ding Liu, Yu Cheng, Chen Fang, Xiaohui Shen, Jianchao Yang, Pan Zhou, and Zhangyang Wang. Enlightengan: Deep light enhancement without paired supervision. *IEEE transactions on image processing*, 30:2340–2349, 2021. 3, 6
- [23] Daniel J Jobson, Zia-ur Rahman, and Glenn A Woodell. Properties and performance of a center/surround retinex. *IEEE transactions on image processing*, 6(3):451–462, 1997. 2
- [24] Daniel J Jobson, Zia-ur Rahman, and Glenn A Woodell. A multiscale retinex for bridging the gap between color images and the human observation of scenes. *IEEE Transactions on Image processing*, 6(7):965–976, 1997. 1, 2
- [25] Edwin H Land. The retinex theory of color vision. *Scientific american*, 237(6):108–129, 1977. 2
- [26] Chulwoo Lee, Chul Lee, and Chang-Su Kim. Contrast enhancement based on layered difference representation of 2d histograms. *IEEE transactions on image processing*, 22(12): 5372–5384, 2013. 1
- [27] Sohyun Lee, Jaesung Rim, Boseung Jeong, Geonu Kim, Byungju Woo, Haechan Lee, Sunghyun Cho, and Suha Kwak. Human pose estimation in extremely low-light conditions. In *Proceedings of the IEEE/CVF Conference on Computer Vision and Pattern Recognition*, pages 704–714, 2023. 1
- [28] Chongyi Li, Jichang Guo, Fatih Porikli, and Yanwei Pang. Lightnetnet: A convolutional neural network for weakly illuminated image enhancement. *Pattern recognition letters*, 104:15–22, 2018. 2
- [29] Risheng Liu, Long Ma, Jiaao Zhang, Xin Fan, and Zhongxuan Luo. Retinex-inspired unrolling with cooperative prior architecture search for low-light image enhancement. In *Proceedings of the IEEE/CVF Conference on Computer Vision and Pattern Recognition*, pages 10561–10570, 2021. 3, 6
- [30] Ze Liu, Yutong Lin, Yue Cao, Han Hu, Yixuan Wei, Zheng Zhang, Stephen Lin, and Baining Guo. Swin transformer: Hierarchical vision transformer using shifted windows. In *Proceedings of the IEEE/CVF international conference on computer vision*, pages 10012–10022, 2021. 4
- [31] Zhuang Liu, Hanzi Mao, Chao-Yuan Wu, Christoph Feichtenhofer, Trevor Darrell, and Saining Xie. A convnet for the 2020s. In *Proceedings of the IEEE/CVF conference on computer vision and pattern recognition*, pages 11976–11986, 2022. 4, 8
- [32] Kin Gwn Lore, Adedotun Akintayo, and Soumik Sarkar. LInet: A deep autoencoder approach to natural low-light image enhancement. *Pattern Recognition*, 61:650–662, 2017. 2
- [33] Ilya Loshchilov and Frank Hutter. Decoupled weight decay regularization. *arXiv preprint arXiv:1711.05101*, 2017. 6
- [34] Feifan Lv, Feng Lu, Jianhua Wu, and Chongsoon Lim. Mbllen: Low-light image/video enhancement using cnns. In *BMVC*, page 4, 2018. 2, 3, 6, 7
- [35] Feifan Lv, Yu Li, and Feng Lu. Attention guided low-light image enhancement with a large scale low-light simulation dataset. *International Journal of Computer Vision*, 129(7): 2175–2193, 2021. 2, 3
- [36] Long Ma, Tengyu Ma, Risheng Liu, Xin Fan, and Zhongxuan Luo. Toward fast, flexible, and robust low-light image enhancement. In *Proceedings of the IEEE/CVF Conference on Computer Vision and Pattern Recognition*, pages 5637–5646, 2022. 3, 6, 7
- [37] Anish Mittal, Rajiv Soundararajan, and Alan C Bovik. Making a “completely blind” image quality analyzer. *IEEE Signal processing letters*, 20(3):209–212, 2012. 6
- [38] Michael K Ng and Wei Wang. A total variation model for retinex. *SIAM Journal on Imaging Sciences*, 4(1):345–365, 2011. 2
- [39] Adam Paszke, Sam Gross, Francisco Massa, Adam Lerer, James Bradbury, Gregory Chanan, Trevor Killeen, Zeming Lin, Natalia Gimelshein, Luca Antiga, et al. Pytorch: An imperative style, high-performance deep learning library. *Advances in neural information processing systems*, 32, 2019. 6
- [40] Stephen M Pizer. Contrast-limited adaptive histogram equalization: Speed and effectiveness stephen m. pizer, r. eugene johnston, james p. ericksen, bonnie c. yankaskas, keith e.

- muller medical image display research group. In *Proceedings of the first conference on visualization in biomedical computing, Atlanta, Georgia*, page 2, 1990. 1
- [41] Olaf Ronneberger, Philipp Fischer, and Thomas Brox. U-net: Convolutional networks for biomedical image segmentation. In *Medical Image Computing and Computer-Assisted Intervention—MICCAI 2015: 18th International Conference, Munich, Germany, October 5-9, 2015, Proceedings, Part III 18*, pages 234–241. Springer, 2015. 3, 5
- [42] Ramprasaath R Selvaraju, Michael Cogswell, Abhishek Das, Ramakrishna Vedantam, Devi Parikh, and Dhruv Batra. Grad-cam: Visual explanations from deep networks via gradient-based localization. In *Proceedings of the IEEE international conference on computer vision*, pages 618–626, 2017. 8
- [43] Xuan Shen, Yaohua Wang, Ming Lin, Yilun Huang, Hao Tang, Xiuyu Sun, and Yanzhi Wang. Deepmad: Mathematical architecture design for deep convolutional neural network. In *Proceedings of the IEEE/CVF Conference on Computer Vision and Pattern Recognition*, pages 6163–6173, 2023. 4
- [44] Christian Szegedy, Vincent Vanhoucke, Sergey Ioffe, Jon Shlens, and Zbigniew Wojna. Rethinking the inception architecture for computer vision. In *Proceedings of the IEEE conference on computer vision and pattern recognition*, pages 2818–2826, 2016. 3
- [45] Li-Wen Wang, Zhi-Song Liu, Wan-Chi Siu, and Daniel PK Lun. Lightning network for low-light image enhancement. *IEEE Transactions on Image Processing*, 29:7984–7996, 2020. 2
- [46] Ruixing Wang, Qing Zhang, Chi-Wing Fu, Xiaoyong Shen, Wei-Shi Zheng, and Jiaya Jia. Underexposed photo enhancement using deep illumination estimation. In *Proceedings of the IEEE/CVF conference on computer vision and pattern recognition*, pages 6849–6857, 2019. 2
- [47] Tao Wang, Kaihao Zhang, Tianrun Shen, Wenhan Luo, Bjorn Stenger, and Tong Lu. Ultra-high-definition low-light image enhancement: a benchmark and transformer-based method. In *Proceedings of the AAAI Conference on Artificial Intelligence*, pages 2654–2662, 2023. 2, 3, 4, 5
- [48] Wenjing Wang, Chen Wei, Wenhan Yang, and Jiaying Liu. Gladnet: Low-light enhancement network with global awareness. In *2018 13th IEEE international conference on automatic face & gesture recognition (FG 2018)*, pages 751–755. IEEE, 2018. 6
- [49] Yufei Wang, Renjie Wan, Wenhan Yang, Haoliang Li, Lap-Pui Chau, and Alex Kot. Low-light image enhancement with normalizing flow. In *Proceedings of the AAAI conference on artificial intelligence*, pages 2604–2612, 2022. 6
- [50] Zhou Wang, Alan C Bovik, Hamid R Sheikh, and Eero P Simoncelli. Image quality assessment: from error visibility to structural similarity. *IEEE transactions on image processing*, 13(4):600–612, 2004. 6
- [51] Zhendong Wang, Xiaodong Cun, Jianmin Bao, Wengang Zhou, Jianzhuang Liu, and Houqiang Li. Uformer: A general u-shaped transformer for image restoration. In *Proceedings of the IEEE/CVF conference on computer vision and pattern recognition*, pages 17683–17693, 2022. 3
- [52] Chen Wei, Wenjing Wang, Wenhan Yang, and Jiaying Liu. Deep retinex decomposition for low-light enhancement. *arXiv preprint arXiv:1808.04560*, 2018. 2, 3, 4, 6
- [53] Wenhui Wu, Jian Weng, Pingping Zhang, Xu Wang, Wenhan Yang, and Jianmin Jiang. Uretinex-net: Retinex-based deep unfolding network for low-light image enhancement. In *Proceedings of the IEEE/CVF conference on computer vision and pattern recognition*, pages 5901–5910, 2022. 2, 6, 8
- [54] Ke Xu, Xin Yang, Baocai Yin, and Rynson WH Lau. Learning to restore low-light images via decomposition-and-enhancement. In *Proceedings of the IEEE/CVF conference on computer vision and pattern recognition*, pages 2281–2290, 2020. 2, 3
- [55] Xiaogang Xu, Ruixing Wang, Chi-Wing Fu, and Jiaya Jia. Snr-aware low-light image enhancement. In *Proceedings of the IEEE/CVF conference on computer vision and pattern recognition*, pages 17714–17724, 2022. 2, 4, 5
- [56] Xiaogang Xu, Ruixing Wang, Chi-Wing Fu, and Jiaya Jia. Snr-aware low-light image enhancement. In *Proceedings of the IEEE/CVF conference on computer vision and pattern recognition*, pages 17714–17724, 2022. 6, 8
- [57] Xiaogang Xu, Ruixing Wang, and Jiangbo Lu. Low-light image enhancement via structure modeling and guidance. In *Proceedings of the IEEE/CVF Conference on Computer Vision and Pattern Recognition*, pages 9893–9903, 2023. 2, 3
- [58] Shuzhou Yang, Moxuan Ding, Yanmin Wu, Zihan Li, and Jian Zhang. Implicit neural representation for cooperative low-light image enhancement. *arXiv preprint arXiv:2303.11722*, 2023. 2, 3
- [59] Syed Waqas Zamir, Aditya Arora, Salman Khan, Munawar Hayat, Fahad Shahbaz Khan, and Ming-Hsuan Yang. Restormer: Efficient transformer for high-resolution image restoration. In *Proceedings of the IEEE/CVF conference on computer vision and pattern recognition*, pages 5728–5739, 2022. 3
- [60] Lin Zhang, Lijun Zhang, Xiao Liu, Ying Shen, Shaoming Zhang, and Shengjie Zhao. Zero-shot restoration of backlit images using deep internal learning. In *Proceedings of the 27th ACM international conference on multimedia*, pages 1623–1631, 2019. 2, 3
- [61] Richard Zhang, Phillip Isola, Alexei A Efros, Eli Shechtman, and Oliver Wang. The unreasonable effectiveness of deep features as a perceptual metric. In *Proceedings of the IEEE conference on computer vision and pattern recognition*, pages 586–595, 2018. 6
- [62] Yukang Zhang and Hanzi Wang. Diverse embedding expansion network and low-light cross-modality benchmark for visible-infrared person re-identification. In *Proceedings of the IEEE/CVF Conference on Computer Vision and Pattern Recognition*, pages 2153–2162, 2023. 1
- [63] Yonghua Zhang, Jiawan Zhang, and Xiaojie Guo. Kindling the darkness: A practical low-light image enhancer. In *Proceedings of the 27th ACM international conference on multimedia*, pages 1632–1640, 2019. 2, 6
- [64] Yonghua Zhang, Jiawan Zhang, and Xiaojie Guo. Kindling the darkness: A practical low-light image enhancer. In *Pro-*

*ceedings of the 27th ACM international conference on multimedia*, pages 1632–1640, 2019. [2](#)

- [65] Anqi Zhu, Lin Zhang, Ying Shen, Yong Ma, Shengjie Zhao, and Yicong Zhou. Zero-shot restoration of underexposed images via robust retinex decomposition. In *2020 IEEE International Conference on Multimedia and Expo (ICME)*, pages 1–6. IEEE, 2020. [3](#), [6](#), [7](#)